Density matrix embedding theory for interacting electron-phonon systems

Barbara Sandhoefer and Garnet Kin-Lic Chan

Phys. Rev. B **94**, 085115 — Published 9 August 2016

DOI: 10.1103/PhysRevB.94.085115

Density matrix embedding theory for interacting electron-phonon systems

Barbara Sandhoefer and Garnet Kin-Lic Chan*
Department of Chemistry, Frick Laboratory, Princeton University, NJ 08544, USA and
Princeton Center for Theoretical Science, Princeton University, NJ 08544, USA
(Dated: June 24, 2016)

We describe the extension of the density matrix embedding theory (DMET) framework to coupled interacting fermion-boson systems. This provides a frequency-independent, entanglement embedding formalism to treat bulk fermion-boson problems. We illustrate the concepts within the context of the one-dimensional Hubbard-Holstein model, where the phonon bath states are obtained from the Schmidt decomposition of a self-consistently adjusted coherent state. We benchmark our results against accurate density matrix renormalization group calculations.

PACS numbers: 71.10.Fd, 74.72.-h, 71.27.+a, 71.30.+h

I. INTRODUCTION

Density matrix embedding theory (DMET) has recently been introduced as an entanglement-based, frequency-independent quantum embedding method for strongly coupled degrees of freedom[1–3]. Similar to the earlier dynamical mean-field theory (DMFT) and its cluster variants[4–7], DMET reformulates a bulk problem as a quantum impurity problem, where the impurity is a subset of the bulk sites. However, unlike DMFT, the impurity embedding is not based on reproducing the lattice Green's function, but rather the entanglement between the impurity and its environment. This time-independent formulation leads to several advantages over the Green's function formulations of DMFT, including a lower computational cost due to the need to describe only stationary states, and the ability to use non-trivial bulk states, for example, with topological order, to describe the entanglement between the impurity and environment. So far, DMET has been applied with significant success to a variety of condensed matter problems in both model and ab-initio settings, e.g. to accurate phase diagrams of the Hubbard model on several lattices[3,8,9]; to frustrated spin systems[10]; to spectral functions[11]; and to compute ab-initio binding curves of bulk materials[12], to name a few examples.

Coupled fermion-boson systems provide a rich setting in which to explore new correlated quantum phases[13]. A prototypical example is a system of electrons interacting with lattice phonons. Such electron-phonon coupling is famously the mechanism for the BCS theory of superconductivity, where Migdal-Eliashberg theory and its generalizations[14–16] provide a quantitative route to transition temperatures and other properties[17,18]. Within this picture the primary effect of the electron-electron interactions is to renormalize the phonon frequency, while the phonons renormalize the electron mass. When stronger Coulomb interactions dominate, however, as is the case in unconventional superconductors such as the cuprates and fullerenes[19,20], the interplay between electron-electron and electron-phonon interactions is less clear. Thus, there is an important demand for numerical methods that can correctly treat both the interacting fermionic degrees of freedom, and the bosonic degrees of freedom, on an equal footing.

In this work, we describe the extension of the DMET framework to treat coupled-fermion boson systems. Strong electron-electron interaction physics are often modeled using an on-site interaction, such as in the Hubbard model, and the prototypical extension to electron-phonon coupling is provided by the Hubbard-Holstein model[21]. While we will not focus here on detailed physics of the Hubbard-Holstein model itself, reserving such a more comprehensive study for future work, we will use this model to illustrate how to extend the DMET framework to treat electron-phonon coupling specifically, and fermion-boson systems more generally. In section II we describe the extension of DMET to electron-phonon problems, using the Hubbard-Holstein model as a concrete example. In section III we provide some illustrate proof-of-concept calculations on the 1D Hubbard-Holstein model, comparing to accurate DMRG calculations. Finally, in section IV we describe the possible extensions of this work such as to coupled fermion-boson systems with interacting bosons.

II. DMET FOR ELECTRON-PHONON SYSTEMS

The Hubbard-Holstein Hamiltonian is defined as

$$H = \sum_{\langle ij\rangle,\sigma} \tilde{t}_{ij} c^\dagger_{i\sigma} c_{j\sigma} + \sum_i U n_{i\alpha} n_{i\beta} + \sum_i \omega_0 \tilde{a}^\dagger_i \tilde{a}_i + \sum_i g n_i (\tilde{a}^\dagger_i + \tilde{a}_i), \quad (1)$$

where $\langle ij\rangle$ denotes nearest neighbours, $c^\dagger_{i\sigma}, \tilde{a}^\dagger_i$ create spin $\sigma \in \{\alpha,\beta\}$-electrons and phonons at site i, respectively, U is the on-site electron-electron interaction, g, the electron-phonon interaction, $\tilde{t}$, the electron hopping and ω_0, the phonon frequency. As is common, we will work in a phonon basis that eliminates the zero-phonon mode through the shift to $a^\dagger_i = \tilde{a}^\dagger_i + \frac{g}{\omega_0}\langle n\rangle$, where $\langle n\rangle = \frac{N_{\mathrm{el}}}{N_{\mathrm{sites}}}$ is the average electronic filling. After this change in basis,

the Hamiltonian becomes, up to a constant,

$$H = \sum_{ij,\sigma} t_{ij} c^\dagger_{i\sigma} c_{j\sigma} + \sum_i U n_{i\alpha} n_{i\beta} + \sum_i \omega_0 a^\dagger_i a_i + \sum_i g(n_i - \langle n \rangle)(a^\dagger_i + a_i), \quad (2)$$

where $t_{ij} = \tilde{t}_{ij} - \frac{2g^2}{\omega_0}\langle n \rangle \delta_{ij}$.

In DMET for ground-states[1–3] the ground-state Ψ and expectation values of an interacting lattice Hamiltonian such as Eq. (2) are approximated by solving for the ground-state of two coupled model problems: a (cluster) impurity model, and an auxiliary non-interacting lattice system. We first introduce these two models in a qualitative fashion. The impurity model with Hamiltonian $H_{\rm imp}$ and ground-state $\Psi_{\rm imp}$, consists of a set of N_c cluster sites (denoted C) cut from the interacting lattice, coupled to N_c bath sites. The bath sites are defined from the auxiliary non-interacting lattice system. The auxiliary lattice Hamiltonian h yields a ground-state Φ, and by performing a Schmidt decomposition between the cluster and the remaining (environment) sites in Φ we obtain a set of bath states. For quadratic h, the Hilbert space of these bath states can be identified with the Hilbert space of a set of *single-particle bath sites* which become the bath sites in the impurity model. The bath sites capture the relevant one-particle physics (e.g. hybridization effects) between the bare cluster and its environment in the impurity problem. Finally, a self-consistency condition links h and $H_{\rm imp}$, where the parameters of h are varied to match the local cluster expectation values of Φ and $\Psi_{\rm imp}$. At convergence, expectation values are defined from $\Psi_{\rm imp}$.

We now illustrate the above general procedure by defining h and $H_{\rm imp}$ precisely for the Hubbard-Holstein model. We first specify h and the construction of the bath sites. In DMET for pure fermionic problems, h is typically chosen as a quadratic fermion Hamiltonian with an associated fermionic Gaussian (Slater determinant[1] or BCS[3]) ground-state Φ. For the Hubbard-Holstein model, we choose h to be the sum of quadratic electron and phonon Hamiltonians

$$h = h_{\rm el} + v_{\rm el} + h_{\rm ph} + v_{\rm ph} + \zeta_{\rm ph} \quad (3)$$

where

$$h_{\rm el} = \sum_{ij,\sigma} t_{ij} c^\dagger_{i\sigma} c_{j\sigma} \quad (4)$$

$$h_{\rm ph} = \sum_i \omega_0 a^\dagger_i a_i + \sum_{\langle ij \rangle} \varepsilon a^\dagger_i a_j - \sum_i g\langle n \rangle (a^\dagger_i + a_i) \quad (5)$$

$$v_{\rm el} = \sum_C \sum_{ij \in C,\sigma} v_{{\rm el},ij} c^\dagger_{i\sigma} c_{j\sigma} \quad (6)$$

$$v_{\rm ph} = \sum_C \sum_{ij \in C} v_{{\rm ph},ij} a^\dagger_i a_j \quad (7)$$

$$\zeta_{\rm ph} = \sum_C \sum_{i \in C} \zeta_{{\rm ph},i} (a^\dagger_i + a_i) \quad (8)$$

and $\sum_C$ denotes summation over the $N_{\rm sites}/N_c$ cluster tiles (with the "impurity" corresponding to $C = 0$), and ε is a constant to be chosen later. The ground-state Φ of h takes the form

$$|\Phi\rangle = |\Phi_{\rm el}\rangle \, |\Phi_{\rm ph}\rangle \quad (9)$$

where $|\Phi_{\rm el}\rangle$ is the ground-state of $(h_{\rm el} + v_{\rm el})$ and is a Slater determinant as in the original DMET while $|\Phi_{\rm ph}\rangle$ is the ground-state of $(h_{\rm ph} + u_{\rm ph} + \zeta_{\rm ph})$.

We use $|\Phi_{\rm el}\rangle$ to define the electronic bath states through its Schmidt decomposition between the impurity cluster and the remaining lattice sites (see the original DMET procedure[1–3])

$$|\Phi_{\rm el}\rangle = \sum_i \lambda_m \, |\alpha_m\rangle \, |\beta_m\rangle \quad (10)$$

where $\{|\alpha_m\rangle\}$, $\{|\beta_m\rangle\}$ denote the impurity and bath many-body Schmidt states. Because of the Gaussian form of $|\Phi_{\rm el}\rangle$, the impurity bath space has the special structure

$$\{|\beta_m\rangle\} = \mathcal{F}(\{d_{i\sigma}\}) \otimes \prod_{j\sigma} e^\dagger_{j\sigma} \, |{\rm vac}_{\rm el}\rangle \quad (11)$$

where $\{d_{i\sigma}\}$ are a set of single-particle bath *orbitals* and $\mathcal{F}$ denotes the corresponding Fock space of these orbitals[2,3]. These bath orbitals together with the impurity cluster sites constitute the electron degrees of freedom in the impurity model, while, in the absence of non-local two-particle, or non-number-conserving interactions, the non-entangled environment orbitals $\{e_{i\sigma}\}$ can be ignored. (This is because for the H under consideration, matrix elements $\langle \alpha_m \beta'_m | H | \alpha_n \beta'_n \rangle$ vanish unless $|\beta'_m\rangle$ and $|\beta'_n\rangle$ have the same set of occupied environment orbitals, and these contribute only a constant term to the energy[3]).

Similarly, $|\Phi_{\rm ph}\rangle$ defines phonon bath states through its Schmidt decomposition. However, if ε in $h_{\rm ph}$ (Eq. (5)) is identically zero, then in this limit the impurity clusters tiling the lattice have no entanglement between them, $|\Phi_{\rm ph}\rangle$ is a product state of the phonon vacuum on each cluster tiling the lattice: $\prod_i |{\rm vac}_{{\rm ph},i}\rangle$, and the bath states are not well defined. For infinitesimal ε, this degeneracy is broken, and in the absence of disorder, the phonons spread through the lattice, creating entanglement. We choose to define ϵ to be 0_+ in this work. Other choices of a degeneracy breaking term are possible. They would lead to slightly different results for a finite cluster size. The choice of this term becomes unimportant as the cluster size is increased, and will only affect the rate of convergence to the infinite cluster limit. $|\Phi_{\rm ph}\rangle$ is then the coherent state

$$|\Phi_{\rm ph}\rangle = \exp z^\dagger \, |{\rm vac}_{\rm ph}\rangle = \exp(-\sum_j z_j a^\dagger_j)|{\rm vac}_{\rm ph}\rangle, \quad (12)$$

$$\text{where } z_j = \sum_{ki} \zeta_k X^T_{ki} \epsilon^{-1}_i X_{ij}.$$

X and ϵ are the eigenvectors and eigenvalues from $\sum_j (\omega_0 \delta_{ij} + \varepsilon_{ij}) X_{jk} = \epsilon_k X_{ik}$.

The Schmidt decomposition of the coherent state Eq. (12) between the impurity cluster $C = 0$ and its environment, can be carried out conveniently by dividing $z^\dagger = \sum_{j \in C=0} z_j a_j^\dagger + z_E^\dagger$, where the first term is on the impurity cluster and the second on the remaining sites. $z_E^\dagger$ defines a single bath orbital, which is a result of the simple structure of the coherent state representation. We can carry out calculations with a single phonon bath orbital, however since the fermionic bath consists of the same number of bath orbitals as there are impurity sites, it seems desirable to obtain a larger set of N_c phonon bath orbitals. To do so, we can further define an artificial division of $z_E^\dagger$ into N_c components through $z_E^\dagger = \sum_{j=1}^{N_c} \tilde{z}_j b_j^\dagger$ and

$$b_j^\dagger = \frac{\sum_{i=(j-1)N}^{jN} z_i a_i^\dagger}{\sum_{i=(j-1)N}^{jN} |z_i|^2}. \tag{13}$$

$N = (N_{\text{sites}} - N_c)/N_c$. The decomposition of Eq. (13) to define additional phonon bath sites is not unique and others can be imagined.

The bath space is then spanned by $\{|\text{vac}_{\text{ph}}\rangle, b_j^\dagger |\text{vac}_{\text{ph}}\rangle, b_i^\dagger b_j^\dagger |\text{vac}_{\text{ph}}\rangle, \ldots\}$, where $\{b_j^\dagger |\text{vac}_{\text{ph}}\rangle\}$ are the phonon bath orbitals. The space of the impurity problem is finally given by the N_c electron and phonon cluster sites, and N_c electron and phonon bath sites. Note that in the above Schmidt decomposition and in the coherent state in Eq. (12) we assume no upper limit on the number of phonons. If, as in the numerical calculations below, we have such a cutoff, the coherent state no longer represents the exact eigenstate of h_{ph}, and the Schmidt decomposition is only approximately represented by the phonon operators in Eq. (13).

With the bath sites at hand, we can now define the impurity Hamiltonian H_{imp}. In DMET, there are two conventions of how to construct the impurity Hamiltonian. The first results in an impurity Hamiltonian of the Anderson type, i.e. the many-particle interactions only appear on the impurity. The second results in an impurity Hamiltonian which has interactions also on the bath sites. Here we use (as previously done in work on lattice Hamiltonians) the first, Anderson impurity construction. Starting from the Anderson-Holstein like lattice Hamiltonian H'

$$H' = h' + \sum_{i \in C=0} U n_{i\alpha} n_{i\beta} + \sum_{i \in C=0} g n_i (a_i^\dagger + a_i), \tag{14}$$

where h' is of the same form as Eq. (3), but with v and ζ terms restricted to sites outside the impurity, i.e. v_{el} is replaced by v'_{el} where

$$v'_{\text{el}} = \sum_{C \neq 0} \sum_{ij \in C, \sigma} v_{\text{el},ij} c_{i\sigma}^\dagger c_{j\sigma}, \tag{15}$$

and $C \neq 0$ excludes summation over the impurity cluster and similarly for v'_{ph} and ζ'_{ph}. Then, the impurity Hamiltonian is given by the projection of H' onto the impurity model space

$$H_{\text{imp}} = P H' P, \tag{16}$$

where P projects onto the space of the impurity model, i.e. $P = \sum_n |\Phi(n)\rangle\langle\Phi(n)|$ where $|\Phi\rangle$ is a product state in the Fock space of the impurity and bath degrees of freedom, and n is an occupancy vector. The projector effects a change of basis from the original electron and phonon basis defined by operators $\{c_i^\dagger\}$, $\{a_i^\dagger\}$, to the cluster plus bath operators, $\{C_i^\dagger\} = \{c_{i\in C=0}^\dagger\} \oplus \{d_i^\dagger\}$, $\{A_i^\dagger\} = \{a_{i\in C=0}^\dagger\} \oplus \{b_i^\dagger\}$. After projection, H_{imp} becomes

$$\begin{aligned} H_{\text{imp}} = &\sum_{ij} T_{ij} C_{i\sigma}^\dagger C_{j\sigma} + \sum_{i \in \text{imp}} U n_{i\alpha} n_{i\beta} + \sum_{ij \in \text{bath}} V_{\text{el},ij} d_{i\sigma}^\dagger d_{j\sigma} \\ &+ \sum_{ij} \Omega_{ij} A_i^\dagger A_j + \sum_{ij \in \text{bath}} \tilde{V}_{\text{ph},ij} b_i^\dagger b_j \\ &+ \sum_{i \in \text{imp}} g(n_i - \langle n \rangle)(a_i^\dagger + a_i) + \sum_{i \in \text{bath}} Z_i (b_i^\dagger + b_i). \end{aligned} \tag{17}$$

where T, Ω, V and Z represent the matrix elements t, ω, v, ζ appearing in h' after projecting into the impurity plus bath site basis, and $n_{i\sigma} = c_{i\sigma}^\dagger c_{i\sigma}$. (Note $i \in$ imp is equivalent to $i \in C = 0$).

Solving the interacting impurity model defined by H_{imp} is much more tractable than the interacting lattice problem. If we enforce a maximum on the phonon number (ph_{max}) then the eigenstate $H_{\text{imp}} |\Psi_{\text{imp}}\rangle = E_{\text{imp}} |\Psi_{\text{imp}}\rangle$ can be obtained straightforwardly by exact diagonalization. This is the impurity solver we use in this work, although other solvers (such as the density matrix renormalization group and coupled cluster theory) have also been employed in DMET[3,8,12].

The last step to specify is the DMET self-consistency, which connects h and H_{imp} and defines v_{el}, v_{ph}, and ζ. These fields are fixed to best match the single-particle electron and phonon density matrices in the impurity problem corresponding to $|\Psi_{\text{imp}}\rangle$ and those of the lattice wavefunction $|\Phi\rangle$. We carry out the minimization of the Frobenius norm of the matrix with elements

$$\Delta\rho_{ij}^{\text{el}} = \langle\Phi|C_i^\dagger C_j|\Phi\rangle - \langle\Psi_{\text{imp}}|C_i^\dagger C_j|\Psi_{\text{imp}}\rangle \tag{18}$$

for the electrons, and

$$\begin{aligned} \Delta\tilde{\rho}_{ij}^{\text{ph}} = &\langle\Phi|a_i^\dagger a_j|\Phi\rangle - \langle\Psi_{\text{imp}}|A_i^\dagger A_j|\Psi_{\text{imp}}\rangle \\ &+ \langle\Phi|A_i^\dagger|\Phi\rangle \delta_{j(2N_c+1)} - \langle\Psi_{\text{imp}}|a_i^\dagger|\Psi_{\text{imp}}\rangle \delta_{j(2N_c+1)} \end{aligned} \tag{19}$$

for the phonons, where i, j run over the impurity and bath sites. The procedure is carried out self-consistently as the new fields lead to a new lattice Hamiltonian h, which leads to new bath sites, a new impurity problem, and a new H_{imp}. The self-consistency can develop multiple branches, which indicates the appearance of new phases.

As with the original fermionic DMET, the electron-phonon DMET constructed above is exact in various limits of the Hubbard-Holstein model. First, it is exact in the limits where the electron-phonon problem is decoupled and ordinary fermionic DMET is exact, i.e. when $U/t \to 0, g \to 0$ (and the interacting lattice H reduces to h) or $U/t \to \infty, g \to 0$ (the atomic limit). It is also exact for $U/t \to 0, g \to \infty$ and $U/t \to \infty, g \to \infty$ as the ground-state wavefunction reduces to the product form in Eq. (9) and the phonon part is a simple product state over localized phonon vacua. Between these various exact limits, the DMET procedure provides a physically motivated interpolation.

III. BENCHMARK STUDIES

We have implemented a pilot version of the DMET electron-phonon formalism above, using an exact diagonalization solver for the impurity problem. To assess the above procedure numerically, we now compute a few benchmarks for the one-dimensional Hubbard–Holstein model. The one-dimensional Hubbard-Holstein model has been the target of extensive numerical studies. Here we will compare to accurate DMRG results on finite chains obtained earlier by Fehske and Jeckelman[22]. In the two limits of $g \to \infty$, $U = 0$ and $g = 0$, $U \to \infty$, it is analytically known that the ground-state is a Peierls insulator and Mott insulator respectively. In the DMRG calculations, the two insulating phases appear with a boundary roughly in the region of $\lambda = \frac{2g^2}{\omega_0} = U$. In addition, Fehske and Jeckelmann observed an intermediate metallic phase which was subdivided into Luttinger liquid and bipolaronic phases. The presence of an intermediate phase in one-dimension is well supported by other numerical studies with various techniques including variable-displacement Lang-Firsov[23], other DMRG studies[24,25], SSE QMC[26,27], and variational Monte Carlo[28]. However, the order of the intermediate phase remains incompletely resolved and depends on the numerical technique used[22,24–26,28].

We first compare the energies obtained from DMET with the DMRG energies of Fehske and Jeckelmann for 14 different parameters of a 32 site 1D Hubbard–Holstein model covering adiabatic ($\omega_0 = 0.5$) and anti-adiabatic ($\omega_0 = 5.0$) regimes, and various values of the coupling $\lambda = 2g^2/\omega_0$ and Hubbard U (all units in t=1). The results are illustrated graphically in Fig. 1 and the detailed energies per site are reported in Table I. The DMRG calculations used open boundary conditions (OBC) and a phonon cutoff of $\mathrm{ph}_{\mathrm{max}} = 8$ phonons per site, while the DMET calculations used a 2-site impurity cluster and anti-periodic boundary conditions (APBC), with the same phonon cutoff. We have also run a small number of points with a larger $\mathrm{ph}_{\mathrm{max}} = 10$ cutoff and find no significant change in the results (e.g. less than 0.01% in the energy). Where indicated in the results, this larger phonon cutoff was used. APBC were used to prevent an exactly

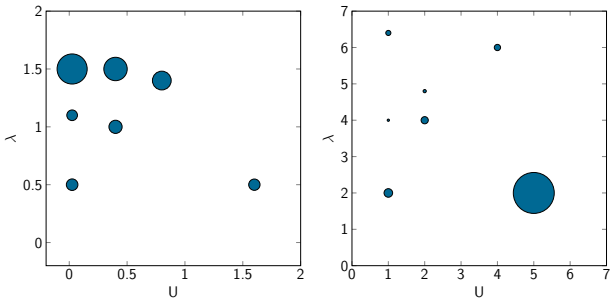

FIG. 1. Errors of the DMET calculation (32 sites, APBC) in percent of the DMRG energy (32 sites, OBC) at different points in the λ, U phase diagram. The radius of the circle is proportional to the relative error. The left panel shows results for the adiabatic regime $\omega = 0.5$, the right panel the anti-adiabatic regime $\omega = 5.0$. For $\omega = 0.5$, the largest energy error is 1.3%, the smallest 0.46%. For $\omega = 5.0$, the largest energy error is 5.63%, the smallest 0.31%. Note that the difference in the APBC and OBC boundary conditions employed in DMET and DMRG calculations itself introduces a 1.9% difference at the free fermion ($U = 0$, $\lambda = 0$) level.

zero gap for the 32-site cluster. Because of the large phonon cutoffs, larger impurity clusters would be costly to solve using the ED solver and are reserved for a future study. The DMET calculations were allowed to break spin symmetry, but not number symmetry. The different boundary conditions mean that we do not expect perfect agreement; in the limit of free fermions ($U = 0$, $\lambda = 0$), the difference between OBC and APBC energies is 1.9%. On this scale, the differences in the DMET and DMRG energies are small and range between 0.5%-5.5% across the parameter ranges. DMET naturally allows a simple extension to larger lattices than 32 sites. In Table I we further show the DMET energies computed over a larger lattice of 504 sites, with the same 2-site impurity and a maximum phonon number $\mathrm{ph}_{\mathrm{max}} = 8$. We see that in this 1D system, the energies are in fact well converged by 32 sites, and change only by about 0.1% going to the larger lattice, with the largest change coming in the itinerant regime. However, as seen in studies on the 2D Hubbard model, we can expect the ability of the DMET to treat larger lattices to become important in higher dimensions, e.g. for the two-dimensional Hubbard-Holstein model[3,8,29,30]. In particular, although only small impurity clusters are studied here, the computational benefits of DMET are clear: for a calculation for twice the size of the impurity model (in this case 4 sites) and with a few (typically $\mathcal{O}(10)$) steps of self-consistency, one obtains a result within 1% of the thermodynamic limit. This advantage is not limited to using ED as solver, but would extend to using other methodologies such as DMRG and QMC as well. The rapid finite size convergence of DMET is particularly useful in gapless systems since the finite impurity cluster is in general not gapless even when the full problem is.

We now study the competition of phases at the cou-

TABLE I. Comparison between DMET (APBC, 2-site cluster) and DMRG (OBC) energies per site for a 32-site Hubbard-Holstein chain with various parameters. $\mathrm{ph}_{\mathrm{max}} = 8$ for all calculations. The difference between APBC and OBC boundary conditions at $U = 0$, $\lambda = 0$ is 1.9%. Additionally DMET energies for 504-site Hubbard-Holstein chain (APBC, 2-site cluster) are also shown.

ω	λ	U	DMRG Energy	DMET Energy (32)	DMET Energy (504)
0.5	1.5	0.025	-2.108	-2.136	-2.136
0.5	1.1	0.025	-1.878	-1.886	-1.886
0.5	0.5	0.025	-1.539	-1.546	-1.545
0.5	1.5	0.4	-2.002	-2.022	-2.022
0.5	1.0	0.4	-1.722	-1.732	-1.730
0.5	1.4	0.8	-1.843	-1.858	-1.857
0.5	0.5	1.6	-1.182	-1.188	-1.188
5.0	6.4	1.0	-6.083	-6.125	-6.125
5.0	4.0	1.0	-3.933	-3.945	-3.945
5.0	2.0	1.0	-2.380	-2.408	-2.407
5.0	4.8	2.0	-4.211	-4.229	-4.229
5.0	4.0	2.0	-3.558	-3.593	-3.588
5.0	6.0	4.0	-4.435	-4.473	-4.470
5.0	2.0	5.0	-1.582	-1.671	-1.671

pling value $\lambda = 4$, in the anti-adiabatic regime, $\omega = 5$. At this coupling value, the DMRG calculations observe three phases: a Peierls insulating phase for $U < 1.5$ and intermediate phase for $1.5 < U < 3.9$, and a Mott insulating phase for $U > 3.9$. As mentioned above, because the DMET calculations do not break number symmetry, we can detect magnetic orders and charge orders, but not superconducting orders. We identify the Peierls phase as a charge-ordered phase with order parameter

$$\Phi_{\mathrm{co}} = \frac{2}{N_c} \sum_{i=0}^{N_c/2} |n_{2i} - n_{2i+1}| \neq 0 \tag{20}$$

and an accompanying charge-excitation gap $\Delta c_1 > 0$ and the Mott phase, as an anti-ferromagnetic (AFM) ordered phase with order parameter

$$\Phi_{\mathrm{afm}} = \frac{1}{N_c} \sum_{i=0}^{N_c} |n_i^{\alpha} - n_i^{\beta}| \neq 0, \tag{21}$$

also and a charge gap. When both orders vanish and there is no gap, we identify the phase as an intermediate phase. In addition to these order parameters, we can also compute a variety of other correlation functions such as the double-occupancy on site 0, $\langle n_0^{\alpha} n_0^{\beta} \rangle$, and the displacement $x_0 = \langle a_0^{\dagger} + a_0 \rangle$. (Note that we use here the single particle gap of the auxiliary lattice system h as a proxy for the charge gap. While not a rigorous measurement it is close to the true single-particle gap in our earlier studies of the Hubbard model on the 1D, honeycomb, and square lattices[1,11]).

In the left panel of Fig. 2 we show the charge-order and AFM order parameters from a set of calculations that sweep from low U to high U, and from high U to low U. These show clear hysteresis, indicating first order phase transitions. The right panel shows the energies of the different DMET coexisting solutions. For $U < 2.5$, the CO (Peierls phase) is lowest in energy. In the region $U = 2.5$ to $U = 4$ CO (and AFM order) is vanishing and a new phase develops. Interestingly, as seen from the middle panel which shows the single-particle gap, in this region the single-particle gap drops to a very small but finite value ($\sim 0.1t$). We identify this phase as the intermediate phase. Similar to as observed in the DMRG studies, the intermediate phase in the DMET calculations does not show charge or magnetic order, but has a small gap rather than being gapless as suggested by the DMRG calculations. It is not clear whether the small gap we observe here would vanish with larger impurity clusters. For $U > 4$ antiferromagnetic order develops, and we enter the Mott insulator phase. In Fig. 3 we show additional observables: the double occupancy, and the displacement. The maximum double occupancy on site 0 is observed in the charge ordered phase and this vanishes as U increases. Similarly we find that the displacement decreases to zero away from the CO phase. Overall, our DMET data closely corresponds to the 3-phase picture in the DMRG calculations, and we observe similar phase boundaries.

IV. CONCLUSIONS

In this work we described the extension of the density matrix embedding theory to systems of coupled fermions and bosons, using the electron-phonon Hubbard-Holstein Hamiltonian as a particular example. We performed pilot calculations on the 1D Hubbard-Holstein model using a small two-site impurity cluster, and found good

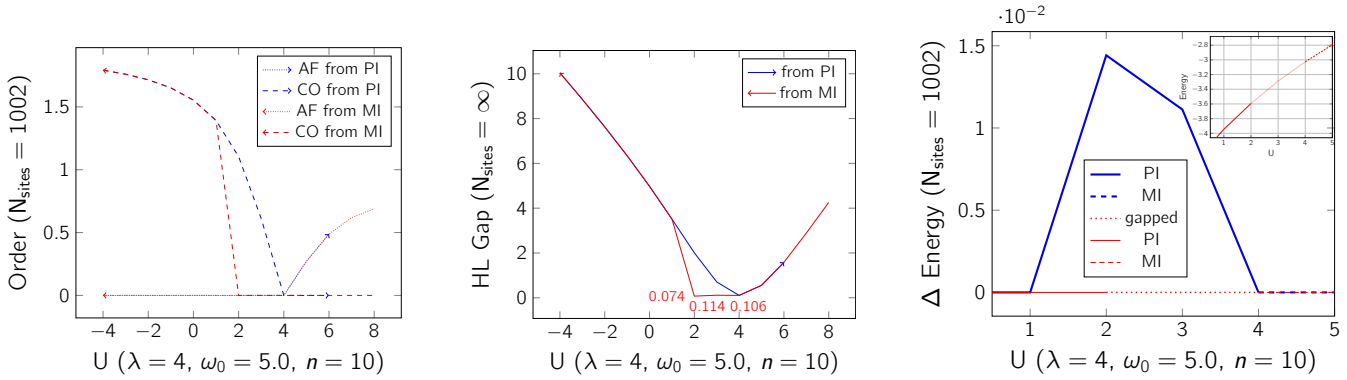

FIG. 2. The left panel shows the transition from the charge-ordered to the spin-ordered phase for $\lambda = 4$ and $\omega = 5.0$. In the forward scan at $U = 4$, the charge-order parameter vanishes, while the anti-ferromagnetic order parameter grows. The backward scan finds a (small) gapped phase without any order parameter for $U = [2, 4]$. The middle panel shows the change of the HOMO-LUMO (auxiliary system single-particle) gap with U. Extrapolation from $N_{\text{sites}} = 102, 502, 1002$ is performed to account for finite-size effects. The different phases are depicted in the right panel (energies given relative to the lowest energy phase). The energy is converged at a maximum phonon number $\text{ph}_{\text{max}} = 10$ and order parameters are given for the chain of length $N_{\text{sites}} = 1002$. Periodic boundary conditions are used throughout.

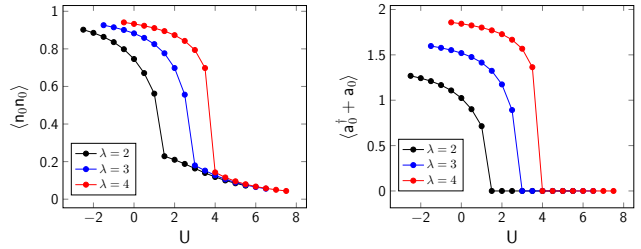

FIG. 3. The left panel shows the double occupancy as a function of U for $\lambda = 2, 3, 4$ and $\omega_0 = 0.5$. The right panel shows the displacement as a function of U. Calculations are carried out with maximum phonon number $\text{ph}_{\text{max}} = 10$ and chain length $\text{N}_{\text{sites}} = 1002$ using periodic boundary conditions.

agreement with the energetics of earlier benchmark DMRG calculations. In the antiadiabatic regime, we also observed a three-phase behaviour, including an intermediate phase between the charge-ordered and Mott-insulating states, with similar phase boundaries as found in the earlier DMRG work.

We can imagine further extensions of the ideas in this report, both respect to the physics and the methodology. For example, here we carried out a preliminary study of the one-dimensional Hubbard-Holstein model. Extending this to studies in two-[30] and higher-dimensions[31,32] is of clear interest. Further, while the Hubbard-Holstein model only contains non-interacting phonons, the DMET formalism is equally applicable to interacting phonons, which would allow us to study many interesting coupled interacting fermion-boson systems, or even interacting pure boson systems, as found, for example in cold atomic gases[13].

With respect to the DMET formulation itself, a key question to explore is alternative definitions of the auxiliary phonon system. While we here used a simple coherent state ground-state to define the phonon bath sites, other choices which describe less classical phonons can be used. Finally, on the numerical front, we employed an exact diagonalization solver for the DMET impurity problem. Extensions to other ground-state solvers, such as the density matrix renormalization group, or diffusion or auxiliary field quantum Monte Carlo, would open up the possibility of more definitive calculations using larger impurities and realistic interactions.

V. ACKNOWLEDGEMENTS

We are grateful to Eric Jeckelmann and Holger Fehske for supplying the DMRG reference energies. We acknowledge helpful discussions with Boxiao Zheng. This work was primarily supported by the US Department of Energy via DE-SC0010530. Additional support was provided by the US Department of Energy, SciDAC DE-SC0008624, as well as through the Simons Foundation, through the Simons Collaboration on the Many-Electron Problem.

* gkchan@princeton.edu

[1] G. Knizia and G. K.-L. Chan, Phys. Rev. Lett. **109**, 186404 (2012).

[2] G. Knizia and G. K.-L. Chan, Journal of Chemical Theory and Computation **9**, 1428 (2013), http://pubs.acs.org/doi/pdf/10.1021/ct301044e.

[3] B.-X. Zheng and G. K.-L. Chan, arXiv preprint arXiv:1504.01784 (2015).
[4] A. Georges, G. Kotliar, W. Krauth, and M. J. Rozenberg, Rev. Mod. Phys. **68**, 13 (1996).
[5] H. Fotso, S. Yang, K. Chen, S. Pathak, J. Moreno, M. Jarrell, K. Mikelsons, E. Khatami, and D. Galanakis, in *Strongly Correlated Systems* (Springer, 2012) pp. 271–302.
[6] T. Maier, M. Jarrell, T. Pruschke, and M. H. Hettler, Reviews of Modern Physics **77**, 1027 (2005).
[7] G. Kotliar, S. Y. Savrasov, G. Pálsson, and G. Biroli, Phys. Rev. Lett. **87**, 186401 (2001).
[8] Q. Chen, G. H. Booth, S. Sharma, G. Knizia, and G. K.-L. Chan, Phys. Rev. B **89**, 165134 (2014).
[9] I. W. Bulik, G. E. Scuseria, and J. Dukelsky, Physical Review B **89**, 035140 (2014).
[10] Z. Fan and Q.-l. Jie, Physical Review B **91**, 195118 (2015).
[11] G. H. Booth and G. K.-L. Chan, Physical Review B **91**, 155107 (2015).
[12] I. W. Bulik, W. Chen, and G. E. Scuseria, The Journal of chemical physics **141**, 054113 (2014).
[13] I. Bloch, J. Dalibard, and W. Zwerger, Rev. Mod. Phys. **80**, 885 (2008).
[14] A. B. Migdal, Sov. Phys. JETP **7**, 996 (1958).
[15] G. M. Eliashberg, Sov. Phys. JETP **11**, 696 (1960).
[16] L. Oliveira, E. Gross, and W. Kohn, Physical review letters **60**, 2430 (1988).
[17] D. Scalapino, J. Schrieffer, and J. Wilkins, Physical Review **148**, 263 (1966).
[18] J. Bauer, J. E. Han, and O. Gunnarsson, Phys. Rev. B **84**, 184531 (2011).
[19] B. Keimer, S. Kivelson, M. Norman, S. Uchida, and J. Zaanen, Nature **518**, 179 (2015).
[20] Y. Takabayashi, A. Y. Ganin, P. Jeglič, D. Arčon, T. Takano, Y. Iwasa, Y. Ohishi, M. Takata, N. Takeshita, K. Prassides, *et al.*, Science **323**, 1585 (2009).
[21] T. Holstein, Ann. Phys. **8**, 325 (1959).
[22] H. Fehske, G. Hager, and E. Jeckelmann, EPL (Europhysics Letters) **84**, 57001 (2008).
[23] Y. Takada and A. Chatterjee, Phys. Rev. B **67**, 081102 (2003).
[24] M. Tezuka, R. Arita, and H. Aoki, Phys. Rev. Lett. **95**, 226401 (2005).
[25] M. Tezuka, R. Arita, and H. Aoki, Phys. Rev. B **76**, 155114 (2007).
[26] R. T. Clay and R. P. Hardikar, Phys. Rev. Lett. **95**, 096401 (2005).
[27] R. P. Hardikar and R. T. Clay, Phys. Rev. B **75**, 245103 (2007).
[28] T. Ohgoe and M. Imada, Physical Review B **89**, 195139 (2014).
[29] J. P. F. LeBlanc, A. E. Antipov, F. Becca, I. W. Bulik, G. K.-L. Chan, C.-M. Chung, Y. Deng, M. Ferrero, T. M. Henderson, C. A. Jimnez-Hoyos, E. Kozik, X.-W. Liu, A. J. Millis, N. V. Prokof'ev, M. Qin, G. E. Scuseria, H. Shi, B. V. Svistunov, L. F. Tocchio, I. S. Tupitsyn, S. R. White, S. Zhang, B.-X. Zheng, Z. Zhu, and E. Gull, Phys. Rev. X **5**, 041041 (2015).
[30] E. Nowadnick, S. Johnston, B. Moritz, R. Scalettar, and T. Devereaux, Physical review letters **109**, 246404 (2012).
[31] G. Sangiovanni, M. Capone, C. Castellani, and M. Grilli, Phys. Rev. Lett. **94**, 026401 (2005).
[32] P. Werner and A. J. Millis, Phys. Rev. Lett. **99**, 146404 (2007).